Progress In Electromagnetics Research, PIER 98, 299–314, 2009

FREQUENCY DOMAIN SKIN ARTIFACT REMOVAL METHOD FOR ULTRA-WIDEBAND BREAST CANCER DETECTION

A. Maskooki, E. Gunawan, C. B. Soh, and K. S. Low

Biomedical Engineering Research Center
Nanyang Technological University
50 Nanyang Drive, Singapore 637553, Singapore

Abstract—Using ultra-wide band (UWB) microwave pulse for breast cancer detection has been greatly investigated recently since it does not expose the patient to any harmful radiation and the implementation is relatively cheaper than other methods such as MRI or X-ray. An issue in UWB imaging of breast cancer is the strong backscatter from the breast skin which is in orders of magnitude larger than the pulse backscattered from the tumor and should be eliminated before processing the signal for the tumor detection and imaging. At present no existing method can effectively remove this artifact without introducing corruption to the tumor signature. In this paper, a novel method to eliminate this artifact is proposed which employs a frequency domain model to isolate and remove skin related information from the signal. This method is compared with the existing methods of the skin artifact removal in different scenarios. The results show that the new method can overcome the shortcomings of the previous methods and improve the detection of the tumor in the sense of the tumor to clutter response ratio.

1. INTRODUCTION

Ultra wide-band (UWB) breast cancer detection has been the subject of investigation in recent years because of its advantages over X-ray mammography. Being noninvasive, using non-ionizing range of electromagnetic waves and avoiding painful breast compression make this method more convenient as a screening tool. This method exploits a confocal microwave imaging (CMI) technique in which a UWB pulse is transmitted from each element of an antenna array sequentially,

Corresponding author: A. Maskooki (arash@pmail.ntu.edu.sg).

and the backscattered signal is collected at the origin. The collected signals are then time shifted and cut according to a synthetic focal point, where all the signal portions received from that point are added to give an estimate of the scattered energy from the focal point. This energy value is then assigned to the pixel value corresponding to that location, hence if there is a strong scatterer at the focal point a high value will be assigned to the pixels corresponding to that vicinity which shows the existence of a lesion in that place.

The received signals consist of mutual couplings between the antenna, skin, and lesions backscatters. Before applying confocal microwave imaging (CMI), antenna coupling effects and skin reflection should be removed from the received signals. Removing the antenna coupling is an instrumental calibration process in which the signal received in the absence of the breast medium is subtracted from the signal in each channel. Eliminating the skin reflection is more complex as this reflection could not be isolated from the other components of the signal as is the case for the antenna coupling. Various methods are proposed in literature to solve the problem. A phantom of the skin-breast interface to imitate the skin reflection and using it to eliminate the skin response is investigated in [1]. However, in practice, making a phantom to exactly reproduce the skin response is very difficult and case dependent. Another simple method to get rid of the unwanted skin artifact is to cut the early time portion of the signal where the skin reflection exists. This seems an easy and effective method at first but the problem arises here is that the tumor response location is not known and may be buried inside another large component of the signal near the skin reflection which gives rise to difficulty of deciding the early time window length and hence there is a risk of removing the tumor reflection partially or completely. Another problem with this method is that it is unable to remove the late time effect of the skin reflection. As reported by [1] using this method will degrade the results. Currently two practical and prevailing skin artifact removal methods exist, which are based on the averaging. The first method as described in [2] simply averages the signals from all channels to remove the skin reflection. The idea is that the skin artifact is assumed to be identical in all channels and hence it will add coherently and appear in the average signal. Therefore, subtracting the average signal of all channel from the signal in each channel will attenuate the skin reflection. But, in practice the skin reflection is not similar in all channels. This is due to the inhomogeneity of the tissue and skin dielectric values and variations in the skin thickness [3]. Hence, practically averaging cannot effectively remove the skin backscatter and, in addition, it causes some deterioration in the tumor signature

as it adds back the tumor response and clutter from the other channels to each response. In [4] a filter, based on the averaging, is proposed to improve the simple averaging. The filter uses a set of coefficients to combine the signals somehow to reduce the mean square error in the early time response of the signal. Although this method improves averaging method, it needs the separation of the early and late time responses which is unknown and also it still deteriorates the signals by adding tumor and clutter reflection from other channels.

The novel method proposed here employs a frequency domain model for the backscattered signal. Using this model the skin related information is eliminated from the frequency domain signal. The signal is then converted back to the time domain and the confocal imaging is applied for the tumor detection. As this method processes each signal individually it does not deteriorate the tumor reflection and adds no clutter from other channels. In addition, this method will remove the skin effect both from early time and late time responses as the skin information is eliminated in frequency domain. Our results show that this method can outperform the averaging based methods in the sense of tumor to clutter response ratio.

2. FREQUENCY DOMAIN MATHEMATICAL MODEL OF THE SIGNAL

As stated in [5] the frequency response of the signal reflected from a number of scattering points could be represented as the sum of a number of complex sinusoids. The number of these terms equals the number of the scattering points in the view of the antenna and multiple scattering effect [6]. In fact, the frequency response could be represented in the following form [7],

$$y(f) = \sum_{i=1}^{N} A_i(f) e^{(j\frac{4\pi}{c}R_i)f} \tag{1}$$

where, f is the frequency, c is the speed of light, N is the number of scattering points and R_i is the range of the ith scattering point. $A_i(f)$ is the frequency dependence function corresponding to the ith scattering point. This frequency dependence function is of the form f^α and the exponent α is known for some common scattering mechanisms [8]. For example, a flat plate has $\alpha = 1$ or a sphere will have $\alpha = 0$ [6]. As stated by Cumo et al. [5], f^α scattering behavior can accurately be estimated by exponential functions over a finite bandwidth interval, so the following discrete model can represent

the frequency behavior of the reflected signal given in (1) above.

$$y(k) = \sum_{i=1}^{N} a_i e^{-(\alpha_i + j\frac{4\pi}{c}R_i)k\Delta f} \tag{2}$$

where a_i are constant coefficients of the sinusoids, α_i and R_i refer to the frequency decay/growth factor and the range of the ith scatterer, respectively, and Δf is the sampling frequency.

3. STATE — SPACE REPRESENTATION OF THE SIGNAL

Now, we will provide the formulation to estimate model parameters in (2) which is described in detail by Piou in [7]. From the system theory we know that the following state-space equations hold for input-output relation in a linear system.

$$\begin{aligned} \mathbf{x}(k+1) &= \mathbf{A}\mathbf{x}(k) + \mathbf{B}\mathbf{w}(k) \\ \mathbf{y}(k) &= \mathbf{C}\mathbf{x}(k) + \mathbf{w}(k) \end{aligned} \tag{3}$$

where $\mathbf{x}(k)$ is the state vector, $\mathbf{w}(k)$ is the input vector and $\mathbf{y}(k)$ is the output of the system. $\mathbf{A}$, $\mathbf{B}$ and $\mathbf{C}$ are matrices characterizing the system and define its state-space behavior. The transfer function of the system described in (3) is given in (4).

$$\mathbf{T}(z) = \frac{\mathbf{Y}(z)}{\mathbf{W}(z)} = \mathbf{C}(z\mathbf{I} - \mathbf{A})^{-1}\mathbf{B} + 1 \tag{4}$$

The impulse response of such system in general comprises a number of complex sinusoids or poles of the system which are the roots of the denominator or as seen in (4) are the eigenvalues of $\mathbf{A}$, the open-loop matrix of the system. Hence, the output signal of the system $y(k)$ can be written as

$$y(k) = \sum_{i=1}^{M} a_i e^{-(\alpha_i + j\beta_i)k\Delta t} \tag{5}$$

In (5) M is the number of the poles of the system or the eigenvalues of $\mathbf{A}$, a_i are the constant coefficients of each complex sinusoid and α_i and β_i are the damping factor and frequency of the ith harmonic, respectively. Δt is the sampling time interval.

Comparing (5) and (2) reveals that the frequency response of the backscattered signal and the impulse response of a linear system have a similar mathematical structure. Thus, we can use the mathematics of linear system identification to estimate the parameters of the frequency

model for the backscattered data. In the rest of this section the formulation to obtain model parameters is presented.

Suppose that the frequency response of the backscattered signal is the impulse response of a hypothetical linear system. Here we try to extract the system matrices and consequently a model for the impulse response based on the eigenvalues or poles of this hypothetical system. As mentioned before we can derive the desired frequency model parameters from this impulse response model.

The process of finding the hypothetical system matrices involves forming forward prediction or Hankel matrix from the sample data of the frequency response of the backscattered signal and deriving $\mathbf{A}$ through singular value decomposition of $\mathbf{H}$, the Hankel matrix which is defined as follows,

$$\mathbf{H} = \begin{pmatrix} y(1) & \cdots & y(L) \\ \vdots & \ddots & \vdots \\ y(N-L+1) & \cdots & y(N) \end{pmatrix} \tag{6}$$

where, $y(i)$ are the samples of frequency domain response of the backscattered data, N is the number of data samples and L is chosen as $N/3$ [9]. By singular value decomposition, $\mathbf{H}$ is decomposed into three matrices,

$$\mathbf{H} = \mathbf{U}\mathbf{\Sigma}\mathbf{V}^* \tag{7}$$

in which $\mathbf{U}$ is the left unitary matrix, $\mathbf{V}^*$ is the right unitary matrix, and $\mathbf{\Sigma}$ is a diagonal matrix containing singular values of $\mathbf{H}$ in a descending order. $(*)$ denotes the complex conjugate and transpose.

Singular values of $\mathbf{H}$ could be separated into two subspaces, the signal plus noise subspace and the only noise subspace. If the SNR value is high enough there would be a sharp transition between singular values of the signal and those of noise. The criterion for separating the two parts is the Akaike information criterion which has been shown to be a reliable model order estimator described in [5, 10]. Hence, $\mathbf{U}$, $\mathbf{\Sigma}$, $\mathbf{V}^*$ could be divided into two different subspaces as follows,

$$\mathbf{H} = [\mathbf{U_{sn}} \quad \mathbf{U_n}] \begin{bmatrix} \mathbf{\Sigma_{sn}} & 0 \\ 0 & \mathbf{\Sigma_n} \end{bmatrix} \begin{bmatrix} \mathbf{V^*_{sn}} \\ \mathbf{V^*_n} \end{bmatrix} \tag{8}$$

which in (8) the subscripts 'sn' and 'n' refer to the signal-noise and noise subspaces respectively. Removing the noise part, $\tilde{\mathbf{H}}$ can be formed as follows,

$$\tilde{\mathbf{H}} = \mathbf{U_{sn}}\mathbf{\Sigma_{sn}}\mathbf{V^*_{sn}} \tag{9}$$

Using the balanced coordinate method [7], $\tilde{\mathbf{H}}$ could further be factorized as

$$\tilde{\mathbf{H}} = \mathbf{\Omega}\mathbf{\Gamma} \tag{10}$$

where

$$\mathbf{\Omega} = \mathbf{U_{sn}}\mathbf{\Sigma_{sn}}^{1/2} \text{ and } \mathbf{\Gamma} = \mathbf{\Sigma_{sn}}^{1/2}\mathbf{V_{sn}^*} \tag{11}$$

where $\mathbf{\Omega}$ and $\mathbf{\Gamma}$ are the observability and controllability matrices respectively. $\mathbf{A}$ could be derived from both the observability or the controllability matrices, here $\mathbf{\Omega}$ is used to derive $\mathbf{A}$.

$$\mathbf{A} = (\mathbf{\Omega^*_{-rl}\Omega_{-rl}})^{-1}(\mathbf{\Omega^*_{-rl}\Omega_{-rf}}) \tag{12}$$

where $\mathbf{\Omega_{-rl}}$ and $\mathbf{\Omega_{-rf}}$ are obtained by removing the last and first rows of $\mathbf{\Omega}$, respectively. Now α_i and R_i are related to the eigenvalues of $\mathbf{A}$ by:

$$\alpha_i = \frac{-\log|\lambda_i|}{\Delta f} \text{ and } R_i = -c\frac{\Phi_i}{4\pi\Delta f} \tag{13}$$

where, as mentioned before, R_i is the range of scattering point and α_i is the damping factor of the sinusoid related to the characteristics of the ith scattering point. Φ_i is the phase of λ_i, the ith eigenvalue of $\mathbf{A}$. To find the constant coefficients a_i we have the equation,

$$a_i = \frac{(\mathbf{Cm_i})(\mathbf{v_iB})}{\lambda_i^{f_1/\Delta f}} \tag{14}$$

where $\mathbf{m_i}$ are eigenvectors of $\mathbf{A}$, and $\mathbf{v_i}$ are defined as

$$\mathbf{V} = [\mathbf{m_1}\cdots\mathbf{m_p}]^{-1} = \begin{bmatrix} \mathbf{v_1} \\ \vdots \\ \mathbf{v_p} \end{bmatrix} \tag{15}$$

In (14), $\mathbf{C}$ is the first row of $\mathbf{\Omega}$, f_1 is the carrier frequency of the pulse and the kth element of frequency vector is related to carrier frequency by

$$f_k = f_1 + (k-1)\Delta f \tag{16}$$

To derive $\mathbf{B}$, $\mathbf{\Omega_N}$ is defined,

$$\mathbf{\Omega_N} = \begin{bmatrix} \mathbf{C} \\ \mathbf{CA} \\ \vdots \\ \mathbf{CA}^{N-1} \end{bmatrix} \tag{17}$$

and $\mathbf{B}$ is obtained by,

$$\mathbf{B} = (\mathbf{\Omega_N^*\Omega_N})^{-1}\left(\mathbf{\Omega_N^*y^T}\right) \tag{18}$$

where $\mathbf{y}$ is the vector of the frequency samples of the backscattered data. Now a_i could be derived from (14). Now that all the parameters of the model in (2) are derived the frequency response of the system could be reconstructed.

4. SKIN SUBTRACTION BY REMOVING SKIN RELATED POLES

This section describes the process of removing skin reflection from the signal using the frequency domain model developed in Section 2. As described in Section 2 each scatterer in the view of the antenna will create a harmonic term in the frequency response of the backscattered signal where each harmonic term consists of a complex exponential and a coefficient. The argument of this complex exponential is the pole of the hypothetical system mentioned in Section 2. By removing the poles corresponding to the skin reflection from the frequency domain signal, all the skin related information will be removed from time domain. The process is as follows.

The received signals are first converted into frequency domain using Fast Fourier Transform (FFT) algorithm. The frequency domain signals are then processed to extract the model parameters stated in the previous section. Among these parameters a_i's are directly related to the amplitudes of each of the backscattered pulses. This can be explained as follows. In Equation (2), a_i is a complex coefficient which can be written as $|a_i|e^{j\theta_i}$ where θ_i is the phase of a_i. Taking the inverse Fourier transform of Equation (2) yields

$$x(t) = \sum_{i=1}^{N} |a_i| \frac{2\alpha_i \cos(\theta_i)}{\alpha_i^2 + (t - 4\pi R_i/c)^2} \tag{19}$$

As seen in Equation (19), $|a_i|$ is proportional to the amplitude of the pulse in the time domain. The backscattered pulse amplitude from the tumor is much smaller than the skin backscatter. Hence, considering this fact a threshold is used to remove poles with dominant a_i values from the frequency response of the signal. Removing the poles over the stated threshold ensures that only the poles corresponding to the skin will be removed from the signal. This will remove the skin effect both in the early time and the late time responses. Hence, the tumor reflection will be preserved without the skin late time response interference in the signal. After removing the skin related poles, the frequency domain signal is reconstructed using the mathematical model (2) and then converted back into the time domain using the inverse-FFT algorithm. Hence, the reconstructed signal will only contain the contributions from tumor and clutter. The clutter will later be rejected using confocal imaging algorithm described in Section 1.

We will first describe the idea in detail using a simplified simulated breast model using SEMCAD X® (version 13) software package for an antenna array with 24 elements in a circular configuration around the breast in order to show the ability of the method to remove the

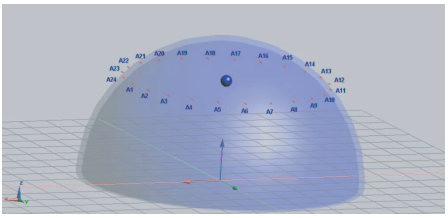

Figure 1. Antenna array and tumor configuration.

Table 1. Antenna arrangement.

Ant. No.	x	y	z	Ant. No.	x	y	z
1	35.71	0	35	13	−35.71	0	35
2	34.50	10.24	35	14	−34.50	−10.24	35
3	30.93	17.86	35	15	−30.93	−17.86	35
4	25.26	26.26	35	16	−25.26	−26.26	35
5	17.86	30.93	35	17	−17.86	−30.93	35
6	9.24	35.50	35	18	−9.24	−35.50	35
7	0	35.71	35	19	0	−35.71	35
8	−9.24	35.50	35	20	9.24	−35.50	35
9	−17.86	30.93	35	21	17.86	−30.93	35
10	−25.50	26.26	35	22	25.26	−26.26	35
11	−30.93	17.86	35	23	30.93	−17.86	35
12	−34.50	10.24	35	24	34.50	−10.24	35

skin reflection from the backscattered signal. The breast medium is modeled by a hemisphere with a radius of 50 mm and thickness of 2 mm as the skin layer. A spherical tumor with a radius of 2 mm is placed on the central axis of the hemisphere and at a height of 35 mm from the center of the hemisphere ($x = 0$ mm, $y = 0$ mm, $z = 35$ mm). The model and the antenna locations are shown in Figure 1 and Table 1 respectively. The relative permittivities of the skin and breast tissues are set to the values given by [11] ($\epsilon_r(skin) = 36$, $\epsilon_r(tissue) = 9$). The dielectric value assigned to the tumor is the measured dielectric value of the malignant tumor $\epsilon_r = 50$ [11]. Figure 2 shows the signal received in channel 1 and its spectrum. As the skin reflects the largest energy among the reflectors in the breast medium, the high energy dominant poles in the frequency domain will correspond to the skin backscatter as it has been discussed in Section 3. Hence a threshold may be used to remove these dominant poles. The threshold is defined based on

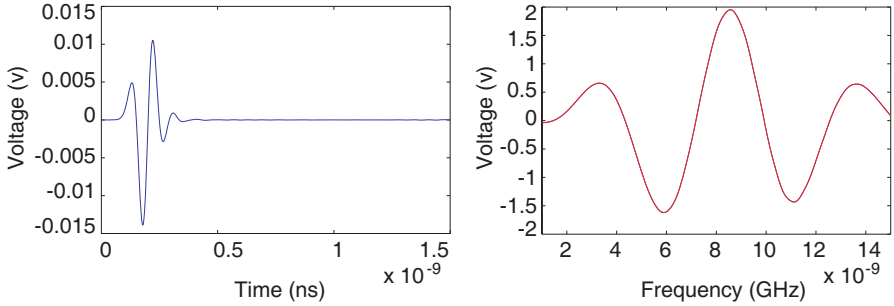

Figure 2. Signal received in channel 1 and its frequency response. (a) Signal received in channel 1. (b) Frequency response of the signal received in channel 1.

the ratio of the backscattered energies of the skin to the tumor and is obtained as follows. We fix the threshold value a little higher than the ratio of the largest possible peak tumor to skin response times the maximum reflection coefficient value a_i which corresponds to the largest scatterer which is the skin surface and remove all the poles with a_i values larger than this threshold from early time response. This way we make sure that only reflections larger than the tumor reflection is removed from the signal. Many factors can affect the skin to tumor response ratio and more study is needed to consider all the factors affecting this ratio and obtain an optimized threshold value. Here, to show the basic idea of the method, we considered three factors, tumor size, skin thickness and tumor location to determine the highest possible ratio. The tumor reflection is isolated from the other reflections by performing two different simulations. One simulation is done without the tumor and the second one is with the tumor. Subtracting the results of these simulations yields the tumor signature. According to [3] breast skin thickness varies in the range of 0.5–3.1 mm; hence two extreme cases (0.5 and 3.1 mm) are simulated in the experiments. The tumor size is set 2 mm and 5 mm which is well within the range of the early breast cancer. Then the tumor location is varied on the line connecting the center to the antenna location from the center of the breast hemisphere to 5 mm below the inner layer of the skin as the tumors so close to the skin can be detected by examining the surface of the breast.

Tables 2 and 3 show the tumor to skin peak response ratio for the skin thickness of 0.5 mm and 3.1 mm respectively.

As expected, the tumor to skin response ratio increases as the

Table 2. Skin to tumor ratio (skin thickness: 0.5 mm).

Location\Tumor size	2 mm	5 mm
Center	9.04E-05	1.81E-04
Under The Skin	3.80E-03	5.20E-03

Table 3. Skin to tumor ratio (skin thickness: 3.1 mm).

Location\Tumor size	2 mm	5 mm
Center	7.72E-05	1.69E-04
Under The Skin	2.10E-03	4.00E-03

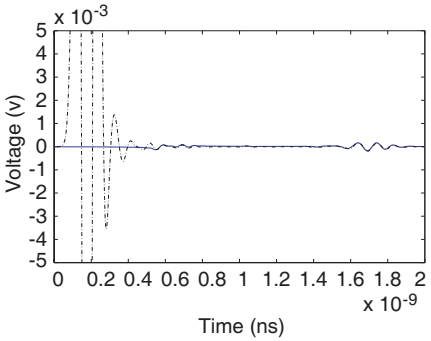

Figure 3. The dotted line shows the original signal and the solid line is the signal after skin backscatter removal.

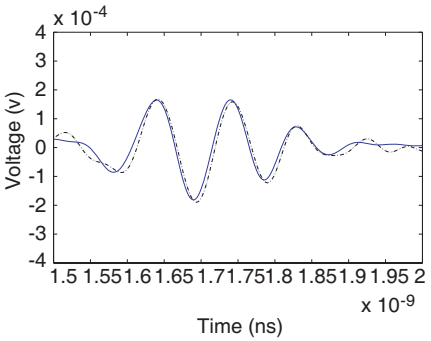

Figure 4. The late time response of the reconstructed signal (line with dots) vs. the original signal (solid).

tumor size increases. As seen in the tables the maximum ratio is obtained when the tumor radius is 5 mm and is located 5 mm below the skin, the highest tumor to skin response ratio is 0.0021, i.e., the skin reflection is about 476 times stronger than the largest tumor reflection. Hence, by setting the threshold a little larger than 0.21% of the largest reflection coefficient ($a_{\max}$) and removing all the poles with a_i values larger than this threshold from early time response we ensure that all the reflections larger than the tumor reflection is removed from the signal. This would be true in all other cases as we chose the largest possible tumor response to define the threshold.

Here, we chose 0.0025 $\times$ the largest reflection coefficient as the threshold value. The poles extracted from the signal in channel 1 are shown in Table 4; Eliminated poles are indicated by a'*'.

Table 4. Reflection coefficients (eliminated poles are identified by *).

Pole No.	Reflection Coefficient	Pole No.	Reflection Coefficient
1	0.006030024	16	0.000576253
2	*0.330168871	17	0.000817322
3	*2.769236715	18	0.001800899
4	*8.978906551	19	0.003023339
5	*17.21322261 (MAX)	20	0.002570893
6	*16.81465757	21	0.000965909
7	*7.610199166	22	0.00044818
8	*1.504612836	23	0.000653675
9	*0.255119890	24	0.001118491
10	*0.052006092	25	0.000111348
11	0.005144400	26	0.00232989
12	0.005526546	27	0.000489255
13	0.004168027	28	0.010678232
14	0.001581127	29	0.022283477
15	0.001108609	30	0.022266937

Figure 3 shows the backscattered signal after removing the skin reflection which is represented using the solid line, super-imposed with the original signal which is represented by the dotted line. Figure 4 shows the late time response of the signals. As seen in Figure 3, the skin reflection is effectively removed from the signal and Figure 4 shows that the rest of the response (the late time response) is not changed significantly.

5. COMPARISON WITH EXISTING METHODS

To compare our method with the averaging [2] and weighted average filter [4] methods, a heterogeneous breast model based on an MRI image shown in Figure 6 is used. The clutter produced due to the heterogeneity of the breast tissue has significant effect on the effectiveness of the skin subtraction methods. In methods which are based on the averaging, when the average of all signals is subtracted from each signal, the averaged clutter response from the other signals is added to the individual signal which will make the tumor detection even more difficult.

As seen in Figure 6 the varying values of the dielectric constants

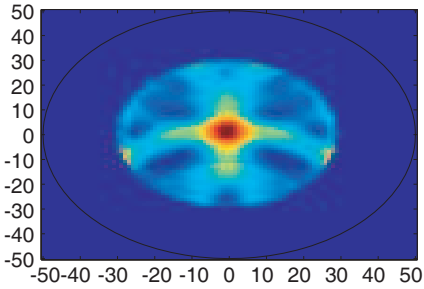

Figure 5. Confocal imaging of the breast after removing the skin reflection.

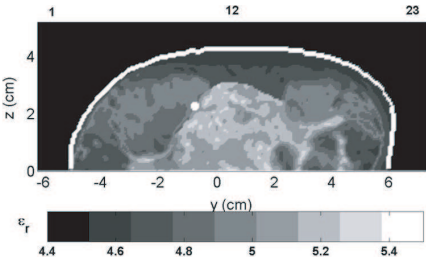

Figure 6. 2D mapping of the dielectric values the different regions of the breast tissue (source: [12]).

Table 5. Dielectric region centers (mm).

Region	x	y	z	ϵ_r	Region	x	y	z	ϵ_r
A	0	0	17	5.3	E	16	10	4	4.8
B	-25	0.9	22	5.2	F	11	-9	11	5
C	-28	26	5	4.8	G	-36	-25	5.5	5
D	4	27	7	4.8	H	27	4.7	22	5.2

of the breast internal regions appear in varying intensities in the gray scale image. The scale for this mapping appears beneath the image. To make our 3D simulation model of the breast medium based on the MRI image, first, we approximate the regions by spheres with radius equal to the circumference of the region divided by 2π. Then the center of the spheres are located at the same height and distance as the center of the corresponding region from the center of the breast. Suppose the vertical axis in Figure 6 is z and the horizontal axis is the x axis in the Cartesian coordinate system. Hence y axis would be on the inward direction perpendicular to the xz plane. To make the model 3D, the angles ϕ_i between the position vectors of the clusters' sphere-centers and x axis are chosen at random in the interval $[-\pi, \pi]$. The tumor is located in ($x = 0$, $y = 0$, $z = 35$ (mm)) in this experiment. Figure 7 shows the model obtained as described above. The locations of the centers of these spheres are given in Table 5.

The skin layer thickness is set to be 2 mm. The antenna placement, physical parameters of the normal breast tissue and tumor are set as described in the previous section. As for the clutter regions, dielectric values are obtained from the MRI image as stated above. These values

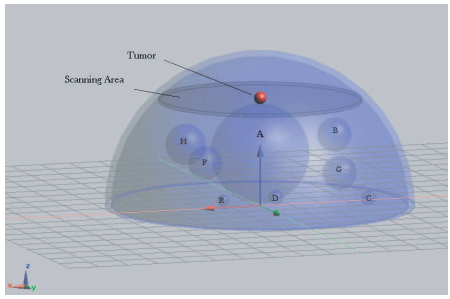

Figure 7. 3D model constructed based on MRI image, shaded region shows the scanning area.

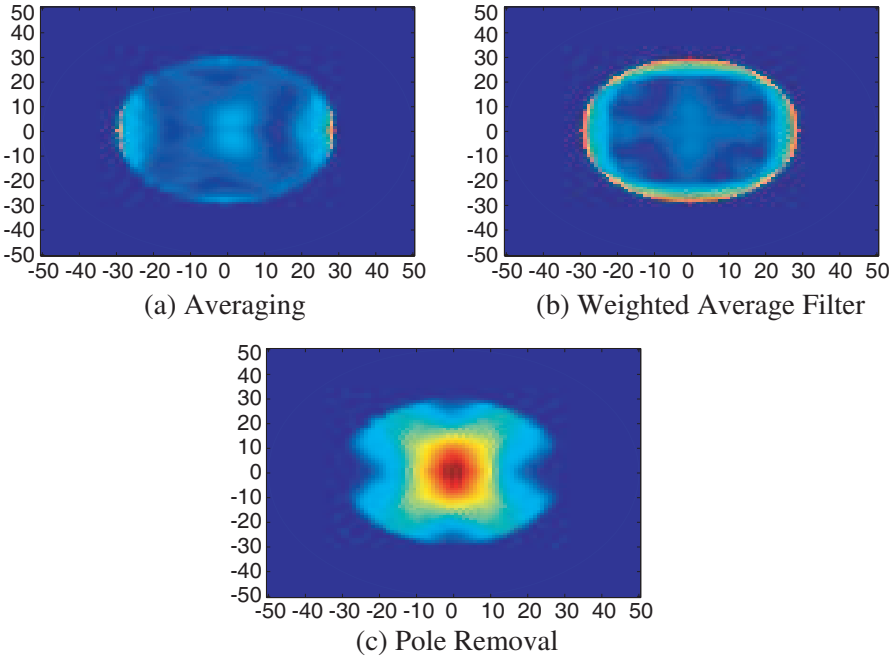

Figure 8. Breast images using three skin subtraction methods: (a) Averaging. (b) Weighted Average. (c) Pole removal.

are given in Table 5.

The signal obtained from simulations are then processed as described in Section 3 to remove the skin contribution from the signal. To compare the effectiveness of this method with the averaging and weighted average filter methods in removing the skin reflection from

the signal, both averaging and weighted average filter are applied on the obtained signal and the 2D image of the breast is formed using confocal imaging process. Figure 8 shows the image obtained from the three methods. As seen in the images from the averaging and weighted average methods, the tumor reflection is removed from the signals, this is because of the symmetry of the tumor location to the antenna elements. During the averaging process in both methods the tumor response is added coherently and appears in the average signal, hence, subtracting the average from the signals will remove the tumor response. But, in the pole removing method each signal is processed separately and no other data is added to or subtracted from the signal, hence, the tumor signature would remain intact. As seen in the figure the tumor is detected at the central axis of the breast.

To investigate the application of the pole removal method in a general case and compare the performance of the three above mentioned methods for any arbitrary tumor location, the tumor is located at $x = 35$, $y = 0$, $z = 15$ (mm). The same model as described above is used for the breast medium.

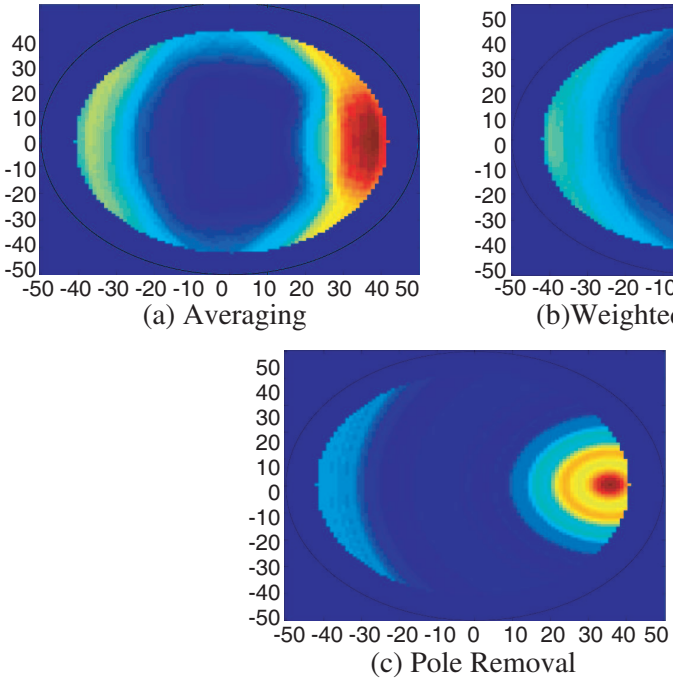

Figure 9. Tumor at: $x = 35$, $y = 0$, $z = 15$ (mm), (a) Averaging. (b) Weighted Average. (c) Pole removal.

Table 6. Tumor to clutter ratio (TCR).

Skin-Removal Method	TCR
Pole-Removal	3.831
Weighted Average	2.082
Averaging	1.837

The skin removing process is performed using the three methods as mentioned in the previous experiment. The resulting images are shown in Figure 9.

The peak response in the figure belongs to the tumor. As seen in the figure all three methods have been successful in removing the skin effect and the tumor is detected in the resulting image. Another peak is resulted by the clutter. We used the Tumor peak to clutter ratio as a criterion to to compare the performance of the methods. Table 6 shows the values achieved by each method. The values show that the averaging has the worst performance and pole removal has the best amongst these methods. This is expected since pole removal method processes each signal individually unlike the other two methods which add clutter from other signals and degrade the tumor reflection.

6. CONCLUSION

In this work we have proposed a new method for removing skin artifact which employs a frequency model to isolate and remove skin related information from the signal. This method is compared with the other two prevailing methods of the skin artifact removal proposed in literature using an MRI based breast model. The results show that the new method can overcome the shortcomings of the previous methods and improve the detection of the tumor in the sense of the tumor to clutter response ratio.

REFERENCES

1. Nilavalan, R., A. Gbedemah, I. Craddock, X. Li, and S. Hagness, "Numerical investigation of breast tumor detection using multi-static radar," *Electronics Letters*, Vol. 39, 1787–1789, 2003.
2. Li, X. and S. Hagness, "A confocal microwave imaging algorithm for breast cancer detection," *IEEE Microwave and Wireless Components Letters*, Vol. 11, No. 3, 130–132, 2001.

3. Ulger, H., N. Erdogan, S. Kumanlioglu, and E. Unur, "Effect of age, breast size, menopausal and hormonal status on mammographic skin thickness," *Skin Research and Technology*, Vol. 9, 284–289, 2003.
4. Bond, E., X. Li, S. Hagness, and B. Van Veen, "Microwave imaging via space-time beamforming for early detection of breast cancer," *IEEE Transactions on Antennas and Propagation*, Vol. 51, No. 8, 1690–1705, 2003.
5. Cuomo, K., J. Piou, and J. Mayhan, "Ultrawide-band coherent processing," *IEEE Microwave Magazine*, Vol. 47, No. 6, 1094–1107, 1999.
6. Moore, T., B. Zuerndorfer, and E. Burt, "Enhanced imagery using spectral-estimation-based techniques," *Lincoln Laboratory Journal*, Vol. 10, No. 2, 171–186, 1997.
7. Piou, J., "A state identification method for 1-D measurements with gaps," *Proc. American Institute of Aeronautics and Astronautics Guidance Navigation and Control Conf.*, Aug. 2005.
8. Keller, J., "A clinical prototype for active microwave imaging of the breast," *IEEE Trans. on Microwave Theory*, Vol. 48, 1841–1853, 2000.
9. Naishadham, K. and J. Piou, "A super-resolution method for extraction of modal responses in wideband data," *IEEE Antennas and Propagation Society International Symposium*, Vol. 4, 4168–4171, 2004.
10. Naishadham, K. and J. E. Piou, "State-space spectral estimation of characteristic electromagnetic responses in wideband data," *IEEE Antennas and Wireless Propagation Letters*, Vol. 4, 406–409, 2005.
11. Fear, E., X. Li, S. Hagness, and M. Stuchly, "Confocal microwave imaging for breast cancer detection: Localization of tumors in three dimensions," *IEEE Transactions on Biomedical Engineering*, Vol. 49, 812–821, 2002.
12. Kosmas, P. and C. Rappaport, "Time reversal with the FDTD method for microwave breast cancer detection," *IEEE Transactions on Microwave Theory and Techniques*, Vol. 53, No. 7, 2317–2322, 2005.